Romanian Reports in Physics, Vol. 61, No. 1, P. 71–93, 2009

CONDENSED MATTER

ON THE EFFECTIVENESS OF VISCOUS DISSIPATION AND JOULE HEATING ON STEADY MHD AND SLIP FLOW OF A BINGHAM FLUID OVER A POROUS ROTATING DISK IN THE PRESENCE OF HALL AND ION-SLIP CURRENTS

EMMANUEL OSALUSI[1], JONATHAN SIDE[2], ROBERT HARRIS[3], BARRY JOHNSTON[4]

[1,2,3] *Renewable Energy Group, International Centre for Island Technology (ICIT), Institute of Petroleum Engineering, Heriot-Watt University, Old Academy, Back Road, Stromness, Orkney KW16 3AW, Scotland, United Kingdom*
Corresponding author: tel. +44(0) 1856 850 605
[4]*Scotrenewables Ltd, Stromness, Orkney KW16 3AW, Scotland, United Kingdom*

(Received February 12, 2007)

Abstract. The combined effects of viscous dissipation and Joule heating on steady magnetohydrodynamics (MHD) and slip flow of an electrically conducting viscous incompressible non-Newtonian Bingham fluid over a porous rotating disk in the presence of Hall and ion-slip currents is studied. An external uniform magnetic field is applied in the z-direction and the fluid is subjected to uniform suction. Numerical solutions are obtained for the governing momentum and energy equations. Results for the details of the velocity as well as temperature are shown graphically and the numerical values of the skin friction and the rate of heat transfer are entered in tables.

Key words: rotating disk, Bingham fluid, Joule heating, viscous dissipation, ion-slip currents.

1. INTRODUCTION

The rotating disk is a popular geometry for studying different fluids, both because of its simplicity and the fact that it represents a classical fluid dynamics problem. Since von Karman [1] elegantly devised a similarity transformation, which reduced the full Navier-Stokes system to a set of ordinary differential equations in a single variable, this swirling flow has received considerable interest; see, e.g., the review by Zandbergen and Dijkstra [2]. Sparrow and Cess [3] examined how the swirling flow caused by a rotating disk is affected by an axial magnetic field, whereas Mitschka and Ulbercht [4] extended von Karman analysis to non-Newtonian fluids.

The fluid that are used extensively in industrial applications are exhibiting a yield stress, that has to be exceeded before the fluid moves. As a result, such fluids cannot sustain a velocity gradient unless the magnitude of the local shear stress is

higher than this yield stress. Fluids that belong to this category include cement, drilling mud, sludge, grease, granular suspensions, aqueous foams, slurries, paints, food products, plastics and paper pulp [5]. Due to the growing use of these non-Newtonian materials in various manufacturing and processing industries, considerable efforts have been directed towards understanding their flow and heat transfer characteristics.

Nomenclature

u	radial velocity, [m/s]
P	pressure, [N/m^2]
g	gravitational acceleration, [m/s^2]
L	characteristic length, [m]
w	axial velocity, [m/s]
Nu	Nusselt number
T	fluid temperature, [K]
B_0	magnetic flux density
c_p	specific heat at constant temperature, [J·kg^{-1}·K^{-1}]
Pr	Prandlt number, $\mu_0 C_p/k_0$
T_w	wall temperature, [C°]
M	magnetic interaction parameter, $\sigma B_0^2/(\rho_0\Omega)$
W	uniform suction/injection, $w/\sqrt{\nu_0\Omega}$
B	Bingham number
υ_0	uniform kinematic viscosity, [m^2/s]
λ	mean free path
φ	tangential axis, [m]
σ^*	Stefan-Boltzmann constant
κ^*	absorption coefficient
$\varnothing$	vertical angle of the disk
η	normal distance from the disk, $z(\Omega/\nu_0)^{1/2}$
Ω	angular velocity, [m/s]
μ	dynamic viscosity, [N_s/m^2]
κ	thermal conductivity coefficient
ρ	fluid density, [kg/m^3]
σ	electrical conductivity
ε	relative temperature different parameter, $\Delta T/T_0$
υ	kinematic viscosity, [m^2/s]
η	dimensional normal distance
τ_t	tangential skin friction
τ_r	radial skin friction
τ_{rz}	radial shear stress
$\tau_{r\varnothing}$	tangential shear stress
γ	slip factor, $[(2-\xi)\lambda\Omega^{1/2}]/\xi\nu^{1/2}$
v	tangential velocity, [m/s]
r	radial axis, [m]
z	vertical axis, [m]
Kn	Knudsen Number
U_t	target velocity, [m/s]
Re	Reynolds number, $\Omega r^2/\nu$
$\mathrm{Re_m}$	magnetic Reynolds number
n	normal direction to the wall
subscript	
w	condition of the wall
0	condition at free stream

Many of the yield non-Newtonian fluids encountered in chemical engineering processes, are known to follow the so-called Bingham model. A Bingham fluid is a material with finite yield stress, followed by a linear curve at a finite strain rate. The yield stress concept was first introduced by Bingham and Gress [6] for a class of fluids known to be viscoplastics fluids. After their initial work, many different equations have been proposed to described the relationship between shear stress and shear rate for different viscoplastic materials (Nguyen and Boger[7]). Many authors ([8-12]) studied the flow or/and heat transfer of a Bingham fluid in different geometries.

Motion of Bingham fluid over a rotating disk has been studied earlier by several authors, e.g.([14, 15, 13]). In these previous investigations, Joule and viscous dissipations were neglected in the energy equation. To the authors' knowledge, no study has yet considered the effects viscous dissipation and Joule heating on MHD flow of a Bingham fluid over a porous rotating disk in the presence of Hall and ion-slip currents.

A completely different extension of von Karmanos one-disk problem is the analysis of Sparrow et al. [3]. They considered the flow of a Newtonian fluid due to the rotation of a porous-surfaced disk and for that purpose replaced the conventional no-slip boundary conditions at the disk surface with a set of linear slip-flow conditions. A substantial reduction in torque then occurred as a result of surface slip. This problem was recently reconsidered by Miklavcic andWang [20] who pointed out that the same slip-flow boundary conditions as those used by Sparrow et al. [3] also could be used for slightly rarefied gases or for flow over grooved surfaces.

The objective of this study is to present the combined effects of viscous dissipation and Joule heating on steady magnetohydrodynamics and slip flow of an electrically conducting viscous incompressible non-Newtonian Bingham fluid over a porous rotating disk. The presence of Hall and ion-slip currents taken into consideration. The governing momentum and energy equations are solve numerically by a shooting method. The inclusion of viscous and Joule heating, the suction, and the non-Newtonian fluid characteristics leads to some interesting effects on both the velocity and temperature fields.

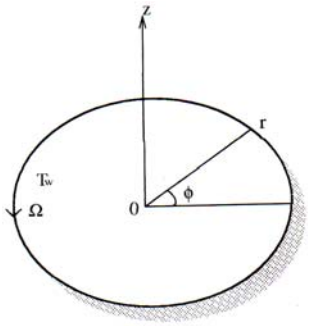

Fig. 1 – Coordinate system for the rotating disk flow.

2. GOVERNING EQUATION

The description of the physical problem closely follows that of Rashaida et al. [14]. We use a non-rotating cylindrical polar coordinate system, (r, φ, z) where z is the vertical axis in the cylindrical coordinates system with r and φ as the radial and tangential axes respectively. The homogeneous, laminar, incompressible electrically conducting Bingham fluid occupies the region $z > 0$ with the rotating disk placed at $z = 0$ and rotating with constant angular velocity Ω. The fluid velocity components are (u, v, w) in the directions of increasing (r, φ, z) respectively, the pressure is P, the density of the fluid is ρ and T is the fluid temperature. The surface of the rotating disk is maintained at a uniform temperature T_w. Far away from the wall, the free stream is kept at a constant temperature T_∞ and at constant pressure P_∞.

An external strong magnetic is applied in the z-direction and has a constant flux density B_0. The magnetic Reynolds number of the flow is taken to be small enough so that the induced distortion of the applied magnetic field can be neglected. The electron-atom collision frequency is assumed to be relatively high, so that the Hall and ion-slip effects cannot be neglected [16]. Assuming the disk to be electrically non-conducting, the generalized Ohm's law gives $j_z = 0$ everywhere in the flow. The governing equations for this investigation are modified to include viscous and Joule heating effects with the generalized Ohm's and Maxwell's laws. The physical model and geometrical coordinates are shown in Fig. 1.

When the boundary layer profile is approximated, the normal strain rates can be neglected in comparison with th shear rates, and when incompressibility and rotational symmetry are taken into account, the constitutive equation of the Bingham fluid becomes [13]

$$\tau_{rz} = \left[\mu_0 + \frac{\tau_y}{\left[\left(\frac{\partial u}{\partial z} \right)^2 + \left(\frac{\partial v}{\partial z} \right)^2 \right]^{1/2}} \right] \frac{\partial u}{\partial z}, \tag{1}$$

$$\tau_{r\phi} = \left[\mu_0 + \frac{\tau_y}{\left[\left(\frac{\partial u}{\partial z} \right)^2 + \left(\frac{\partial v}{\partial z} \right)^2 \right]^{1/2}} \right] \frac{\partial v}{\partial z}. \tag{2}$$

Then the equations governing the motion of the steady MHD flow of the Bingham fluid over a porous rotating disk can be stated as

$$\frac{\partial u}{\partial r}+\frac{u}{r}+\frac{\partial w}{\partial z}=0, \tag{3}$$

$$\rho\left(u\frac{\partial u}{\partial r}+\frac{v^2}{r}+w\frac{\partial u}{\partial z}\right)+\frac{\partial P}{\partial r}=\frac{\partial}{\partial r}\left(\mu\frac{\partial u}{\partial r}\right)+\frac{\partial}{\partial r}\left(\mu\frac{u}{r}\right)+\frac{\partial \tau_{rz}}{\partial z}-\frac{\sigma B_0^2}{\alpha^2+\beta_e^2}\left(\alpha u-\beta_e v\right), \tag{4}$$

$$\rho\left(u\frac{\partial v}{\partial r}+\frac{uv}{r}+w\frac{\partial v}{\partial z}\right)=\frac{\partial}{\partial r}\left(\mu\frac{\partial v}{\partial r}\right)+\frac{\partial}{\partial r}\left(\mu\frac{v}{r}\right)+\frac{\partial \tau_{r\Phi}}{\partial z}-\frac{\sigma B_0^2}{\alpha^2+\beta_e^2}\left(\alpha v-\beta_e u\right), \tag{5}$$

$$\rho c_p\left(u\frac{\partial T}{\partial r}+w\frac{\partial T}{\partial z}\right)=\kappa\frac{\partial^2 T}{\partial z^2}+\frac{\sigma B_0^2}{\alpha^2+\beta_e^2}\left(u^2-v^2\right)+\mu\left[\left(\frac{\partial u}{\partial z}\right)^2+\left(\frac{\partial v}{\partial z}\right)^2\right], \tag{6}$$

where, $\sigma\left(=\left(e^2 n_e t_e\right)/m_e\right)$ is the electrical conductivity, e is the electron charge, t_e is the electron collision time, n_e is the electron number density, and m_e is the mass of the electron. c_p is the specific heat at constant pressure of the fluid, $\alpha=1+\beta_i\beta_e$, $\beta_e\left(=\omega_e t_e\right)$ is the Hall parameter with $\omega_e\left(=eB_0/m_e\right)$ is the electron frequency, and $\beta_i\left(=en_eB_0/\left(\left(1+n_e/n_a\right)K_{ai}\right)\right)$ is the ion-slip parameter, n_a is the neutral particle number density, and K_{ai} is the friction coefficient between ions and neutral particles.

The second and third terms on the RHS of equation (6) denote the magnetic and viscous heating terms, respectively.

When the mean free path of the fluid particles is comparable to the characteristic dimensions of the flow field domain, Navier-Stokes equations break down since the assumption of continuum media fails. In the range 0.1 < Kn < 10 of Knudsen Number, the high order continuum equations, e.g. Burnett equations should be used. For the range of 0.1 < Kn < 10.001, no-slip boundary conditions can not be used and should be replaced with the following expression (Ga-el-Hak [21]):

$$U_t=\frac{2\psi}{\psi}\lambda\frac{\partial U_t}{\partial n}, \tag{7}$$

where U_t is the target velocity, n is the normal direction to the wall, ψ is the target momentum accommodation coefficient λ and is the mean free path. For Kn < 0.001, the no-slip boundary condition is valid, therefore, the velocity at the surface is equal to zero. In this study the slip and the no-slip regimes of the Knudsen number that lies in the range 0.1 > Kn > 0 is considered. By using equation (7), the boundary conditions are introduced [22] as follows:

$$\begin{aligned} &u = \frac{2-\xi}{\xi}\lambda\frac{\partial u}{\partial z}, \qquad v = r\Omega + \frac{2-\xi}{\xi}\lambda\frac{\partial v}{\partial z} \qquad w = W, \qquad T = T_w, \quad \text{at} \quad z = 0 \\ &u \to 0, \quad v \to 0 \qquad T \to T_w, \quad P \to P_\infty \qquad \text{as} \quad z \to \infty. \end{aligned} \tag{8}$$

3. SIMILARITY TRANSFORMATION

The solutions of the governing equations are obtained by introducing a dimensionless normal distance from the disk, $\eta = z\left(\Omega/\upsilon_0\right)^{1/2}$ along with the von-Karman transformations,

$$\begin{aligned} &u - \Omega r F(\eta), \qquad v = \Omega r G(\eta), \qquad w = \left(\Omega\upsilon_0\right)^{1/2} H(\eta) \\ &P - P_0 = 2\mu_0\Omega p(\eta) \quad \text{and} \quad T - T_0 = \left(T_w - T_0\right)\theta(\eta), \end{aligned} \tag{9}$$

where υ_0 is a uniform kinematic viscosity of the fluid. Substituting these transformations into equations (1)-(6) gives the nonlinear ordinary differential equations,

$$H' + 2F = 0, \tag{10}$$

$$\begin{aligned} &F''\left[1 + \frac{2\mathrm{B}}{\left(F'^2 + G'^2\right)^{1/2}} - \frac{2\mathrm{B}F'^2}{\left(F'^2 + G'^2\right)^{3/2}}\right] - \frac{2\mathrm{B}F'G'G''}{\left(F'^2 + G'^2\right)^{3/2}} - \\ &-\left[F^2 - G^2 + F'H\right] - \left[\frac{M}{\left(\alpha^2 + \beta_e^2\right)}\left(\alpha F - \beta_e G\right)\right] = 0, \end{aligned} \tag{11}$$

$$\begin{aligned} &G''\left[1 + \frac{2\mathrm{B}}{\left(F'^2 + G'^2\right)^{1/2}} - \frac{2\mathrm{B}G'^2}{\left(F'^2 + G'^2\right)^{3/2}}\right] - \frac{2\mathrm{B}F'G'F''}{\left(F'^2 + G'^2\right)^{3/2}} - \\ &-\left[2F^2G + HG'\right] - \left[\frac{M}{\left(\alpha^2 + \beta_e^2\right)}\left(\alpha G - \beta_e F\right)\right] = 0, \end{aligned} \tag{12}$$

$$\frac{\theta''}{\mathrm{Pr}} - H\theta' + \frac{\mathrm{Ec}M}{\alpha^2 + \beta_e^2}\left(F^2 + G^2\right) + \mathrm{Ec}\frac{(1+2\mathrm{B})\left(F'^2 + G'^2\right)}{\left(F'^2 + G'^2\right)} = 0, \tag{13}$$

where: $\mathrm{B} = \tau_y / \left(2\rho\Omega r \left(\upsilon_0 \Omega\right)^{1/2}\right)$ is a Bingham number [13], $\upsilon_0 = \mu_0 / \rho$ is the kinematic viscosity of the plastic fluid, $\mathrm{Pr} = \mu_0 c_p / \kappa$ is the Prandtl number, $M = \sigma B_0^2 / (\rho\Omega)$ is the magnetic interaction parameter that represents the ratio of the magnetic force to the fluid inertial, $\mathrm{Ec} = \left(r^2\Omega^2\right) / \left[\left(T_w - T_0\right) c_p\right]$ is the Eckert number. A prime symbol denotes a derivative with respect to η. The transformed boundary conditions are given by;

$$F = \gamma F', \qquad G = 1 + \gamma G', \qquad H = W, \qquad \theta = 1 \quad \text{at} \quad \eta = 0 \tag{14}$$

$$F = G = \theta = p = 0, \qquad \text{at} \qquad \eta \to \infty, \tag{15}$$

where $\gamma = \left[\left(2 - \xi\right)\lambda\Omega^{1/2}\right] / \xi\upsilon^{1/2}$ is the slip factor, $W = w / \sqrt{\upsilon_\infty \Omega}$ represents a uniform suction ($W < 0$) or injection ($W > 0$) at the surface. The boundary conditions (15) imply that both the radial (F), the tangential (G), temperature and pressure vanish sufficiently far away from the rotating disk, whereas the axial velocity component (H) is anticipated to approach a yet unknown asymptotic limit for sufficiently large η-values.

The skin friction coefficients and the rate of heat transfer to the surface are given by:

$$\tau_t = \left[\mu\left(\frac{\partial v}{\partial z} + \frac{1}{r}\frac{\partial w}{\partial \phi}\right)\right]_{z=0} = \mu_0 \left[1 + \frac{2\mathrm{B}}{\left(F'(0)^2 + G'(0)^2\right)^{1/2}}\right] \mathrm{Re}^{1/2}\Omega G'(0),$$

and

$$\tau_r = \left[\mu\left(\frac{\partial u}{\partial z} + \frac{1}{r}\frac{\partial w}{\partial r}\right)\right]_{z=0} = \mu_0 \left[1 + \frac{2\mathrm{B}}{\left(F'(0)^2 + G'(0)^2\right)^{1/2}}\right] \mathrm{Re}^{1/2}\Omega F'(0),$$

Hence the tangential and radial skin-frictions are respectively given by

$$\mu_0 \left[1 + \frac{2\mathrm{B}\mu_0}{\left(F'(0)^2 + G'(0)^2\right)^{1/2}}\right]^{-1} \mathrm{Re}^{1/2} C_{f_t} = G'(0), \tag{16}$$

and

$$\mu_0\left[1+\frac{2B\mu_0}{\left(F'(0)^2+G'(0)^2\right)^{1/2}}\right]^{-1}\mathrm{Re}^{1/2}C_{f_t}=F'(0). \tag{17}$$

Fourier's law

$$q=-\kappa\left(\frac{\partial T}{\partial z}\right)_{z=0}=-\kappa\left[\frac{\Omega}{\upsilon}\right]^{1/1}\theta'(0), \tag{18}$$

is used to calculate the rate of heat transfer from the disk surface to the fluid. The Nusselt number Nu is obtained as

$$R^{-1/2}\mathrm{Nu}=-\theta'(0), \tag{19}$$

where $\mathrm{Re}\left(=\Omega r^2/\upsilon\right)$ is the rotational Reynolds number and $\upsilon=\mu_0/\rho$ is the kinematic viscosity of the plastic fluid.

4. METHOD OF SOLUTION

The systems of nonlinear ordinary differential equations (10)-(13) is solved under the condition given in (15) for the three components of the flow velocity and temperature distribution, using the shooting method ([18, 19]). The resulting system of first order equations has to be solved in the infinite domain $0 < \eta < 1$. A finite domain in the η-direction can be used instead with η chosen large enough to ensure that the solutions are not affected by imposing the asymptotic conditions at a finite distance. The dependence of the results from the length of the finite domain was ensured and successfully checked by various trial and error numerical experimentations. Table 1 demonstrates these numerical experiments in evaluating the axial flow at infinity H_∞ for various values of the Hall parameters β_e and using a finite distances η_∞. As clear from the table that $\eta_\infty = 51$ is adequate and therefore, computations are carried out based on this value.

5. NUMERICAL RESULTS AND DISCUSSION

For numerical computations, we took Pr = 0.72, which is the value of Prandtl number for air. We have confined our analysis to the case when we have suction velocity only, that is, when $W < 0$. Table 2 displays the numerical results for $F'(0), -G'(0)$ and $-\theta'(0)$ for different values of $\gamma, \mathrm{B}, M, \mathrm{Ec}, \beta_e$ and β_i. Inspection of Table 2 reveals that a moderate increase in the value of the slip factor

may lead to a gradual monotonic decrease in the radial $\left(F'(0)\right)$ and tangential $\left(G'(0)\right)$ skin-friction coefficient, while it increases the rate of heat transfer $\left(\theta'(0)\right)$ coefficient.

Table 1

H_∞	η_∞=21	η_∞=26	η_∞=51
M=1 β_e=0.0	–1.08289006	–1.082890067	–1.082890067
M=1 β_e=0.1	–1.10355391	–1.103553920	–1.103553920
M=1 β_e=0.2	–1.12341251	–1.123412510	–1.123412510

Table 2

Numerical values of $F'(0), -G'(0)$ and $\theta'(0)$ for various values of γ, B, M, Ec, β_e and β_i with Pr = 0.72 and W = –1

γ	B	M	Ec	β_e	β_i	F'	G'	$-\theta'(0)$
0.1	1.0	1.0	0.2	0.1	0.1	0.289980639490150	1.214972265229669	0.783604096854857
0.2	1.0	1.0	0.2	0.1	0.1	0.197089246924161	1.092359539897380	0.810197609034829
0.3	1.0	1.0	0.2	0.1	0.1	0.140589646472720	0.985420877408089	0.828702975780790
0.4	1.0	1.0	0.2	0.1	0.1	0.104240627873361	0.895233324308893	0.842274784815356
0.1	0.0	1.0	0.2	0.1	0.1	0.233512810375559	1.109185921507533	0.834659734383682
0.1	1.0	1.0	0.2	0.1	0.1	0.080102976634553	1.035288488474593	0.618772240397839
0.1	2.0	1.0	0.2	0.1	0.1	0.047954642243222	1.017767386500090	0.419019083851568
0.1	3.0	1.0	0.2	0.1	0.1	0.034201652218587	1.009926381023437	0.221740117967231
0.1	0.1	0.0	0.2	0.1	0.1	0.191285566408897	1.098259466225487	0.847569131507427
0.1	0.1	1.0	0.2	0.1	0.1	0.197089246924161	1.092359539897380	0.810197609034829
0.1	0.1	2.0	0.2	0.1	0.1	0.202871483120214	1.086553104591176	0.772863931682586
0.1	0.1	3.0	0.2	0.1	0.1	0.208501442952224	1.080923921258974	0.735517371239731
0.1	0.1	1.0	0.2	0.1	0.1	0.197089247256380	1.092359539866416	0.966588854882803
0.1	0.1	1.0	0.2	0.1	0.1	0.197089247094142	1.092359539929945	0.888393231900400
0.1	0.1	1.0	0.2	0.1	0.1	0.197089246924161	1.092359539897380	0.810197609034829
0.1	0.1	1.0	0.2	0.1	0.1	0.197089246769944	1.092359539789066	0.732001986326178
0.1	0.1	1.0	0.2	0.0	0.1	0.165897761396752	1.116968238407230	0.805471781764924
0.1	0.1	1.0	0.2	0.1	0.1	0.197089246924161	1.092359539897380	0.810197609034829
0.1	0.1	1.0	0.2	0.2	0.1	0.226644472510622	1.069325077694991	0.815397880179770
0.1	0.1	1.0	0.2	0.3	0.1	0.253368469976243	1.048776423878241	0.820795146622949
0.1	0.1	1.0	0.2	0.1	0.0	0.197459790423797	1.092055722293216	0.809491162497113
0.1	0.	11.0	0.2	0.1	0.1	0.197089246924161	1.092235953989380	0.810197609034829
0.1	0.1	1.0	0.2	0.1	0.2	0.196731014890602	1.092653417509087	0.810882566966077
0.1	0.1	1.0	0.2	0.1	0.3	0.196384612240423	1.090937742217997	0.811549831161616

Table 2 reveals that a moderate increase in the value of the B may lead to a gradual monotonic decrease in theradial $F'(0)$, tangential $-G'(0)$ skin-friction and the rate of heat transfer $-\theta'(0)$ coefficient respectively. In Table 2 we noticed that an increase in M increases $F'(0)$ but decreases both $-G'(0)$ and $-\theta'(0)$. This is due to the fact that magnetic field reduces the radial F (Fig. 2a), but increases the tangential velocity G (Fig. 2b) and temperature θ (Fig. 2d). Further, we observe that radial skin friction $F'(0)$, tangential skin friction $-G'(0)$ and the rate of heat transfer $-\theta'(0)$ decrease with Ec. Also, an increase in the values of Hall parameter β_e increases both the shear stress in the radial $F'(0)$ direction and the rate of heat transfer $-\theta'(0)$ coefficient while increase in the value of β_e decreases shear stress in the tangential $-G'(0)$ direction. Table 2 reveals that as ion-slip parameter β_i increases, the radial skin friction $F'(0)$ decreases with an increase in both tangential skin friction $-G'(0)$ and rate of heat transfer coefficient $-\theta'(0)$ increases respectively.

The shear-driven flow (G) in the tangential direction in Fig. 2b is gradually reduced with increasing values of γ. The centrifugal force associated with this circular motion causes the outward radial flow (F), which is correspondingly reduced with decreasing slip coefficient close to the disk surface. The radial outflow F is compensated by an axial inflow H towards the rotating disk, in accordance with the mass concentration equation (10). The gradual reduction of the peak in the F-profiles in Fig. 2a with decreasing values of γ is reflected in the distributions of the axial velocity component in Fig. 2c. The distinct inflection point in the H-profiles for the highest values of γ seems to gradually disappear with increasing slip. This is a consequence of the direct coupling between the radial and axial velocity components through the continuity constraint (10). The reduction of the radial velocity $F(\eta)$ with decreasing γ automatically gives rise to a reduced axial inflow since

$$-H(\infty) = 2\int_0^\infty F\mathrm{d}\eta. \tag{20}$$

Figure 2d shows the temperature profile. A general decrease in temperature profile is observed with maximum at the disk surface and minimum far away from the disk. The magnitude of the temperature profiles decreases slightly with increase in slip coefficient.

Similarity solutions for three velocity components (radial, tangential and axial) and the temperature are presented in Figures 3a-3d for values of the

Bingham number B in the range of 1 to 3. Figure 2a depicts the representative radial velocity F distributions. It is noted that F decreases as the strength of Bingham number increases. Since the radial velocity is zero at both the surface of the disk and in the far field, there must be a maximum value somewhere in between. The profile of the radial velocity F becomes flatter as the value of B is increased, i.e. the maximum velocity decreases, and its location moves slightly further from the disk. For $B > 0$, the radial outflow must carry away the incoming axial flow with an apparent viscosity now consisting of two parts, i.e., the Bingham plastic viscosity and the yield stress. Thus, the level of the radial velocity $-H$ component decreases (Fig. 3c) with increasing B and also persists a longer distance from the disk before it vanishes. Fig. 3b shows the tangential velocity G profiles. It is readily seen from Fig. 3b that G increases with B. The temperature θ profiles is shown in Fig. 3d. We noticed that an increase in Bingham number B increases the temperature θ. This is due to the fact that increase in Bingham number increases the yield stress and in turn increases the viscous dissipation of the fluid.

Figures 4a–4d show typical profiles for the fluid radial velocity F, tangential velocity G, axial velocity $-H$ and temperature θ for different values of the magnetic parameter M, respectively. Due to the damping effect of the magnetic field, increases in the values of M have a tendency to slow the motion of the fluid in radial F, tangential G and axial $-H$ directions and make it warmer as it moves over the disk causing the temperature θ to increase.

Figures 5a–5d show the F, G, $-H$ and θ profiles for various values of β_e between 0 and 0.3. We observe that radial velocity F, tangential velocity G and axial velocity $-H$ increase while the temperature θ decreases as the Hall current parameter β_e increases since the magnetic damping on F, G and $-H$ decreases as β_e increases coupled with the fact that magnetic field has a propelling effect on F, G and $-H$.

Figures 6a–6d describe the behaviour of F, G and θ with changes in the values of the ion-slip parameter β_i. From Figs. 6a–6d, it is clear that an increase in the ion-slip parameter β_i leads to a decrease in the radial velocity F, tangential velocity G, axial velocity $-H$ and temperature θ. In general, it is noted that, the effect of Hall parameter β_e on the flow and thermal fields is more notable than that of ion-slip parameter β_i. This is attributed to the fact that the diffusion velocity of the electrons is much larger than that of ions.

Figure 7 illustrates the temperature θ profiles for various values of Ec between 0 and 0.3. It is noticed that temperature θ increases with Eckert number Ec. The rise in the temperature θ is due to the heat created by the increase in viscous dissipation and compression work ($Ec \neq 0$).

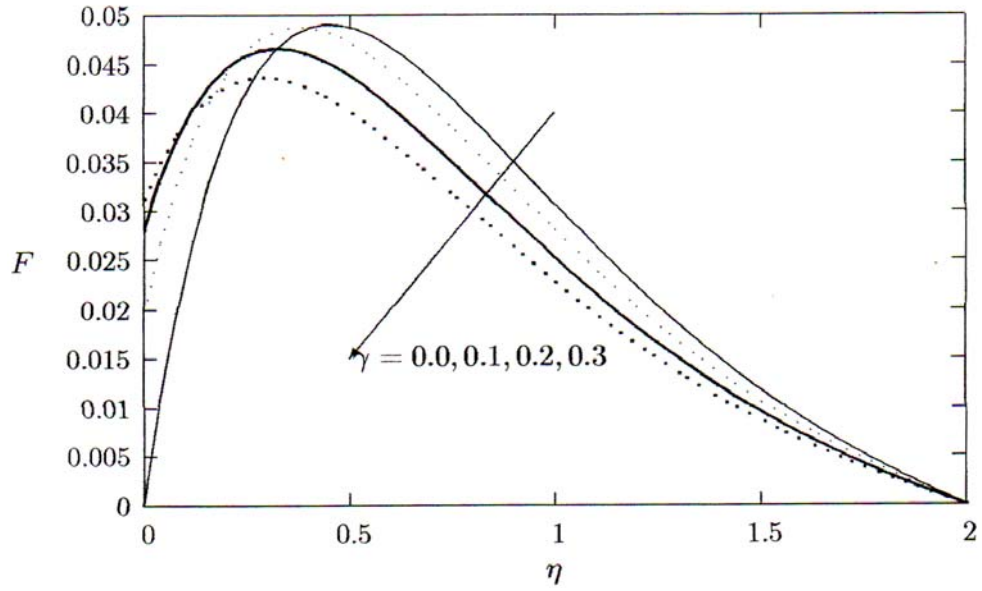

a

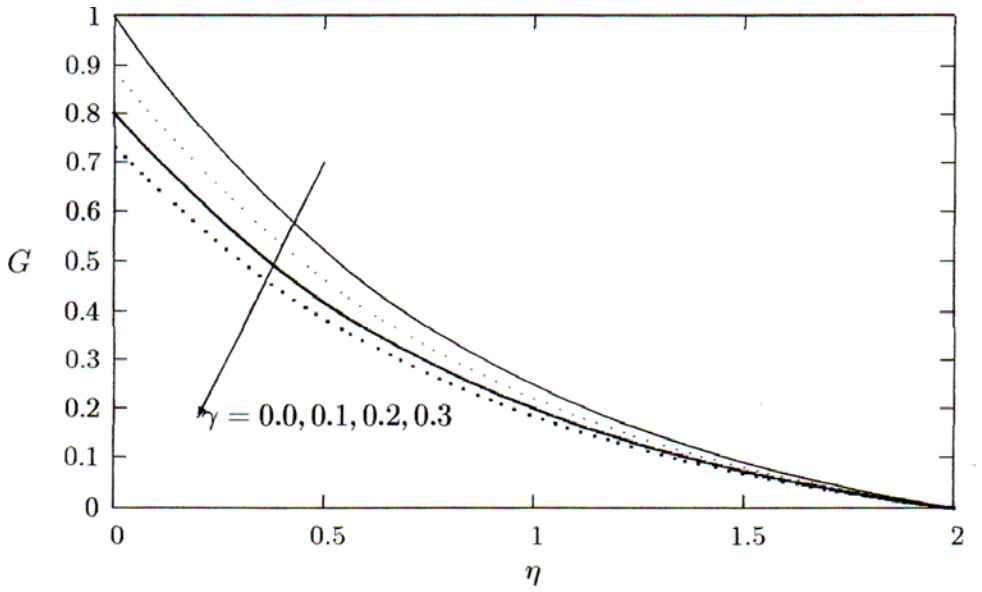

b

Fig. 2a,b – Effect of γ on the radial velocity profiles (a) and on the tangential velocity profiles (b), for: B = 0.1, Ec = 0.2, Pr = 0.72, $\beta_e = 0.1$, $\beta_i = 0.1$, $M = 1$ and $W = -1$.

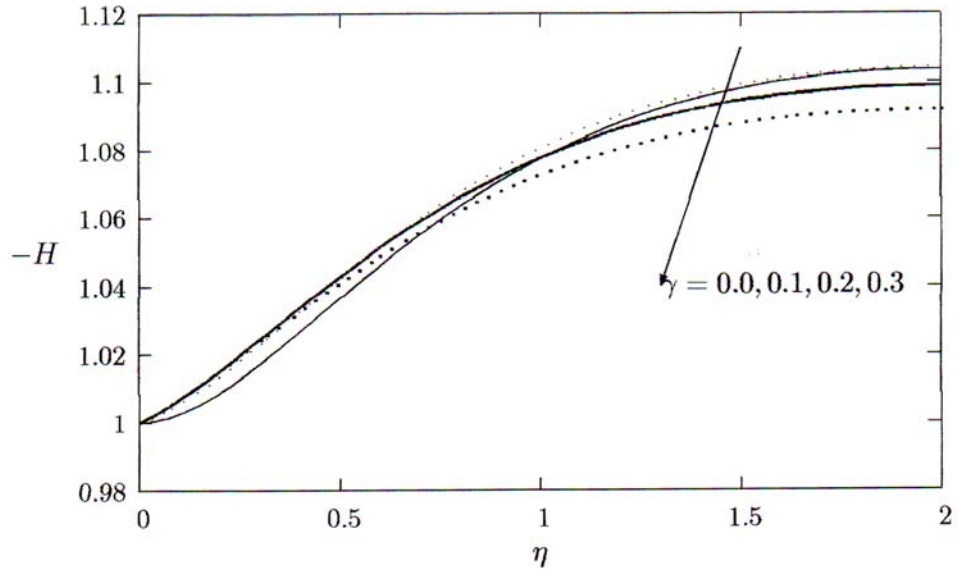

c

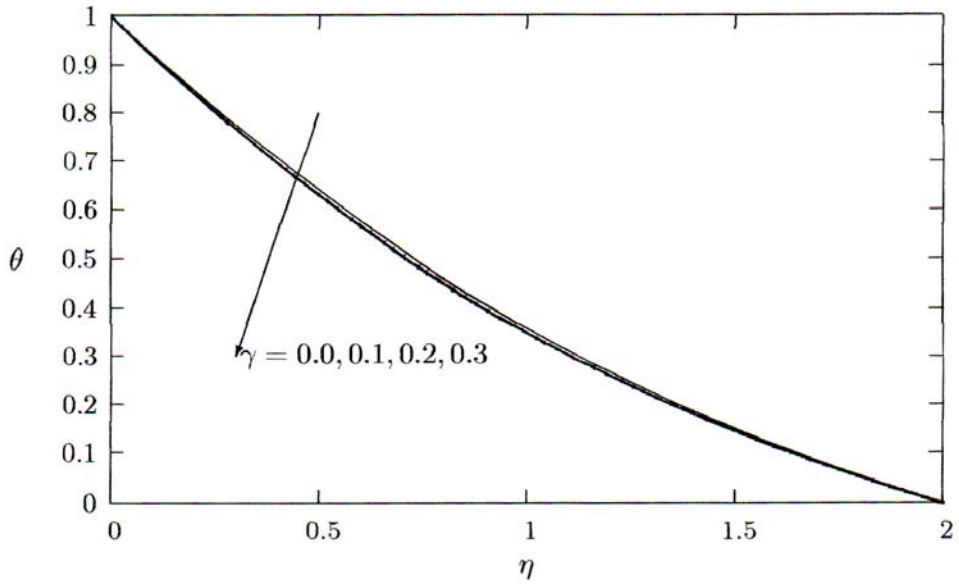

d

Fig. 2c,d – Effect of γ on the axial velocity profiles (c) and on the temperature profiles (d), for: B = 0.1, Ec = 0.2, Pr = 0.72, $\beta_e = 0.1$, $\beta_i = 0.1$, $M = 1$, and $W = -1$.

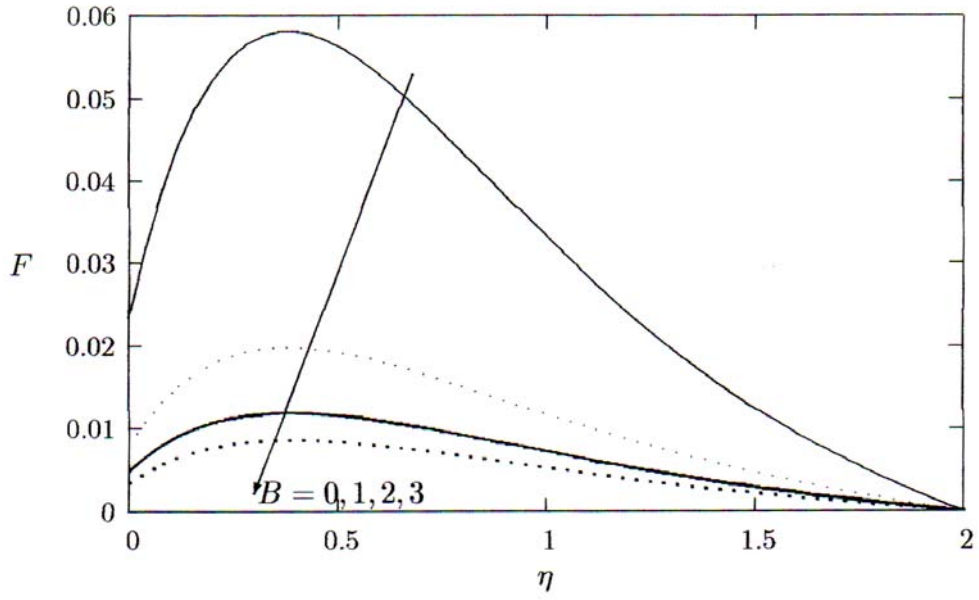

a

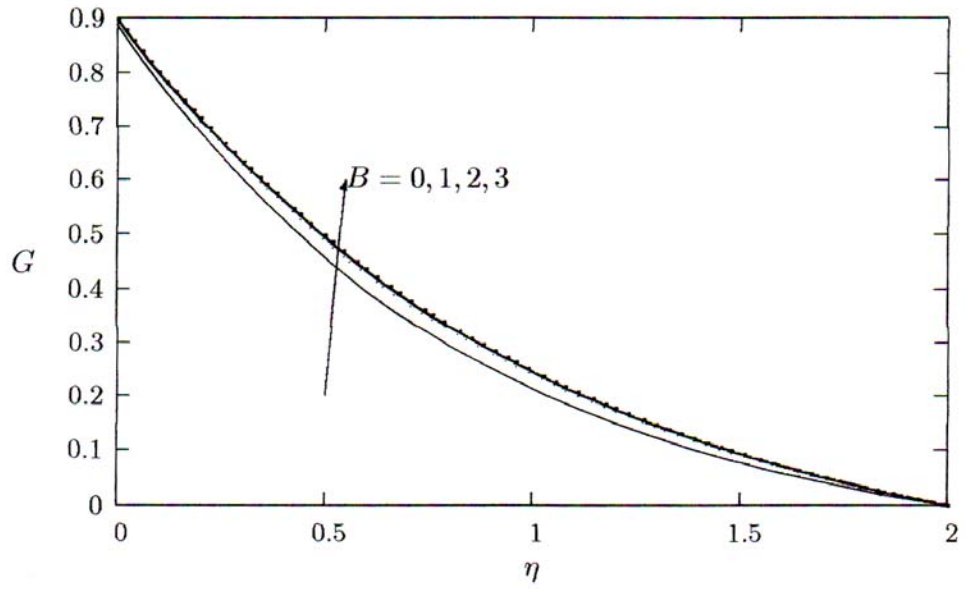

b

Fig. 3a,b – Effect of B on the radial velocity profiles (a) and on the tangential velocity profiles (b), for: Ec = 0.2, Pr = 0.72, $\gamma = 0.1$, $\beta_e = 0.1$, $\beta_i = 0.1$, $M = 1$ and $W = -1$.

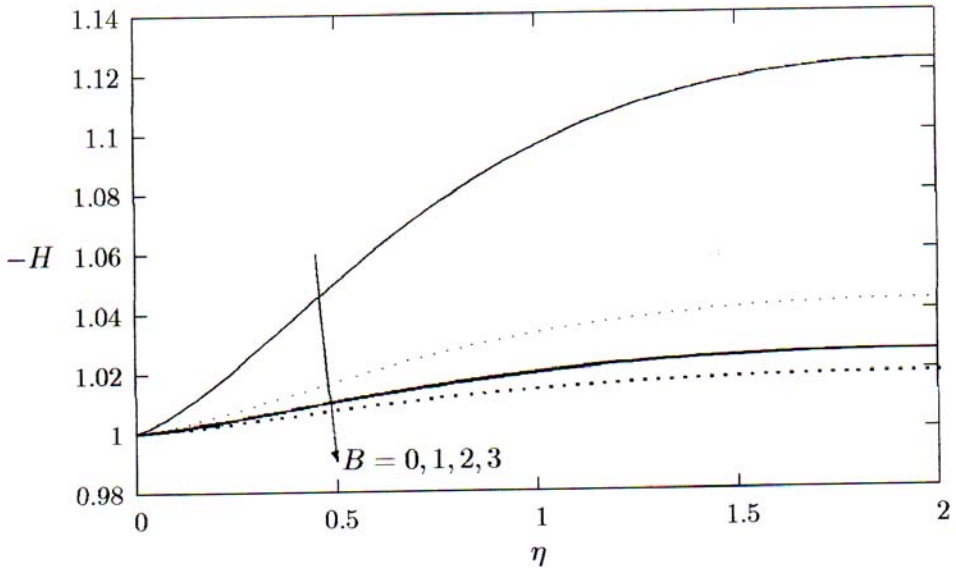

c

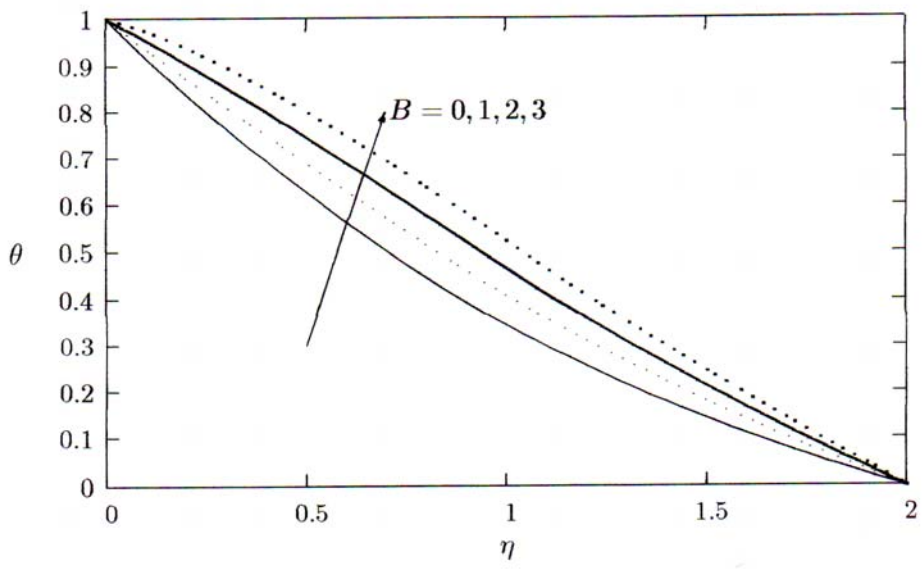

d

Fig. 3c,d – Effect of B on the axial velocity profiles (c) and on the temperature profiles (d), for: Ec = 0.2, Pr = 0.72, $\gamma = 0.1$, $\beta_e = 0.1$, $\beta_i = 0.1$, $M = 1$ and $W = -1$.

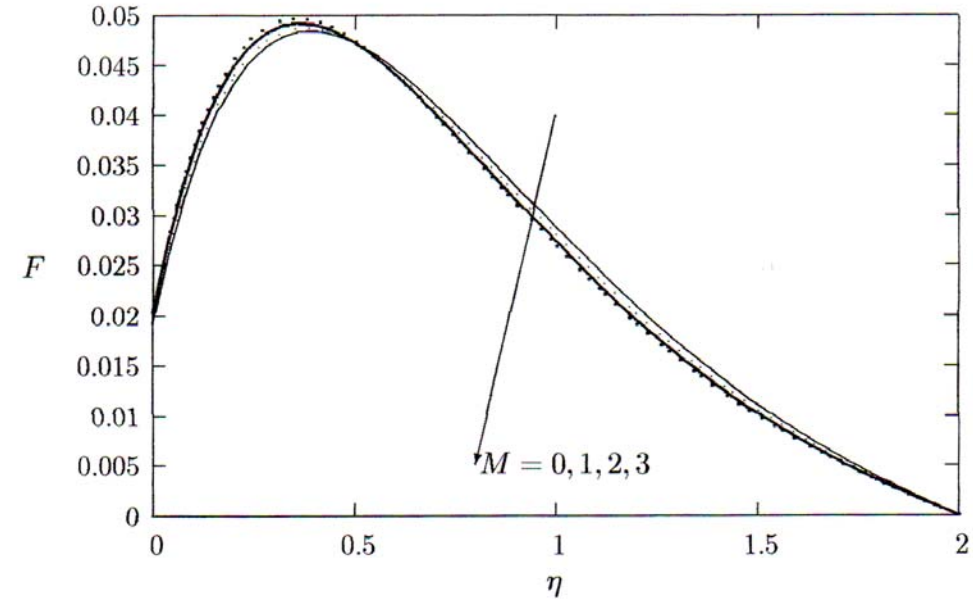

a

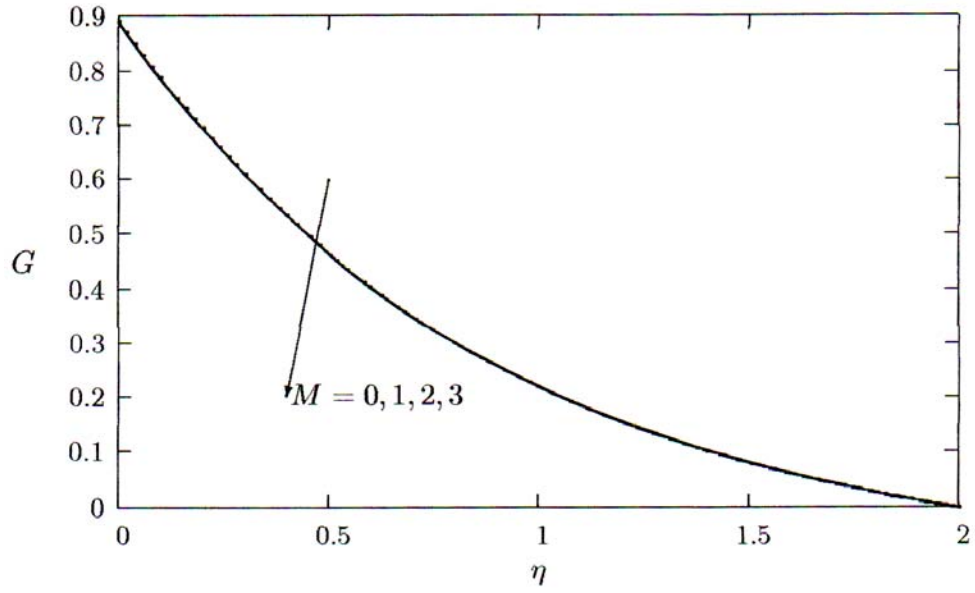

b

Fig. 4a,b – Effect of M on the radial velocity profiles (a) and on the tangential velocity profiles (b), for: Ec = 0.2, Pr = 0.72, $\gamma = 0.1$, $\beta_e = 0.1$, $\beta_i = 0.1$, B = 0.1, and $W = -1$.

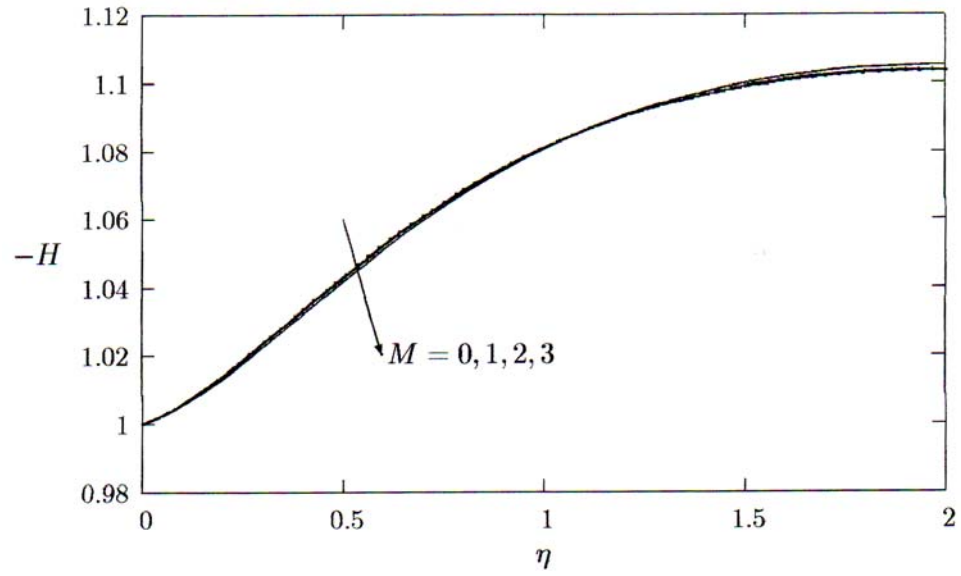

c

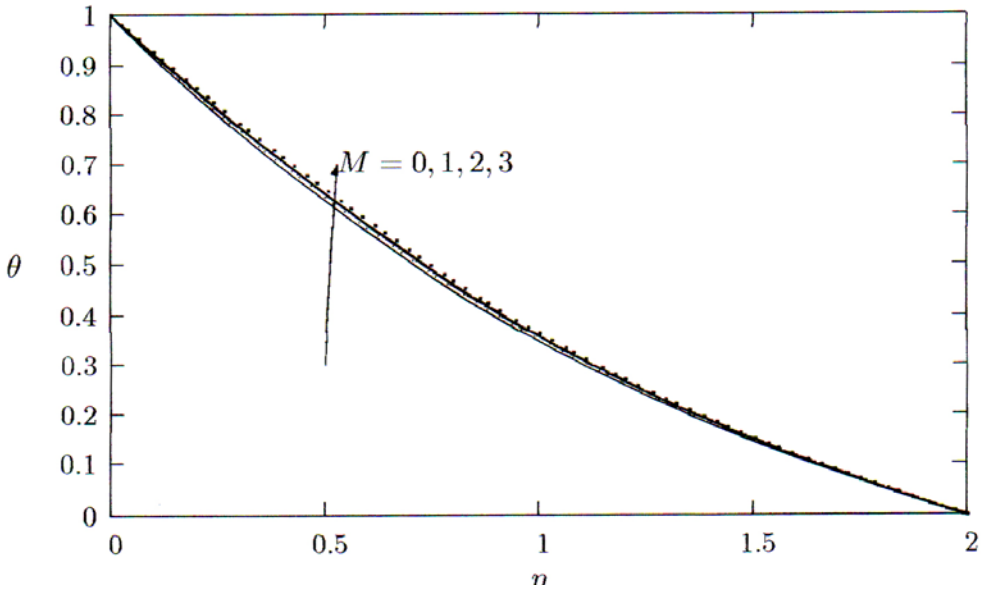

d

Fig. 4c,d – Effect of M on the axial velocity profiles (c) and on the temperature profiles (d), for: Ec = 0.2, Pr = 0.72, $\gamma = 0.1$, $\beta_e = 0.1$, $\beta_i = 0.1$, B = 0.1, and $W = -1$.

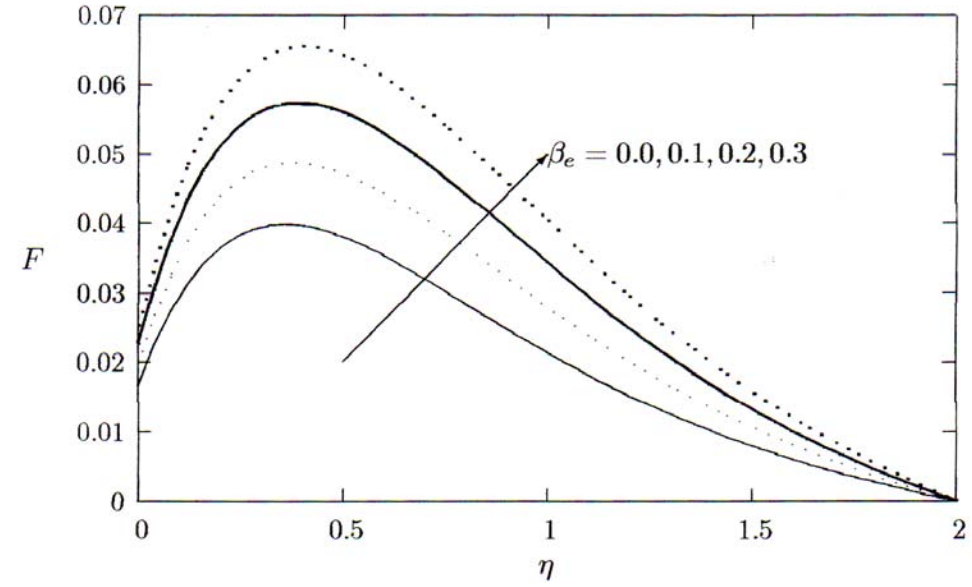

a

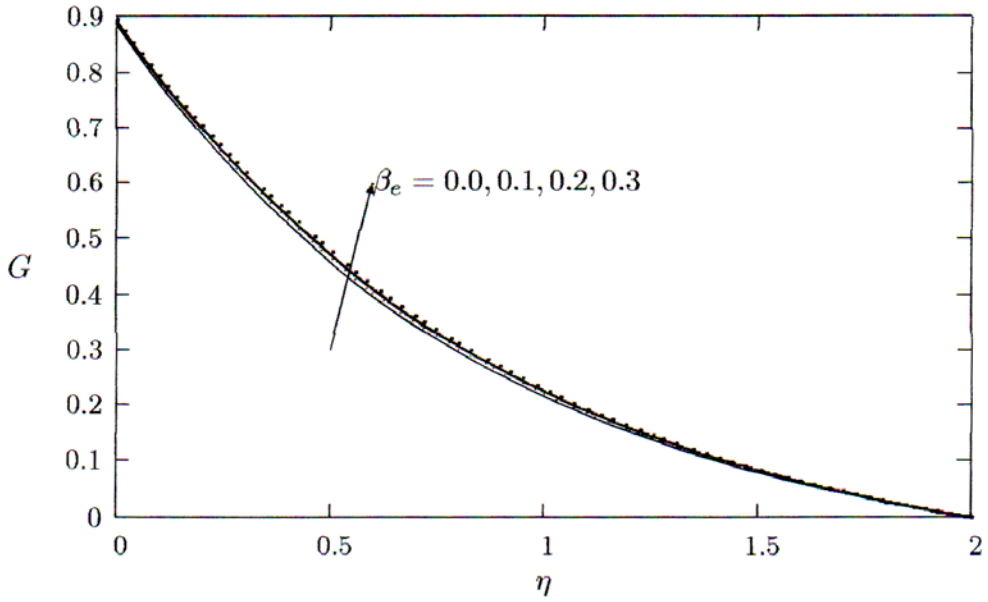

b

Fig. 5a,b – Effect of β_e on the radial velocity profiles (a) and on the tangential velocity profiles (b) for: Ec = 0.2, Pr = 0.72, $\gamma = 0.1$, $M = 1$, $\beta_i = 0.1$, B = 0.1, and $W = -1$.

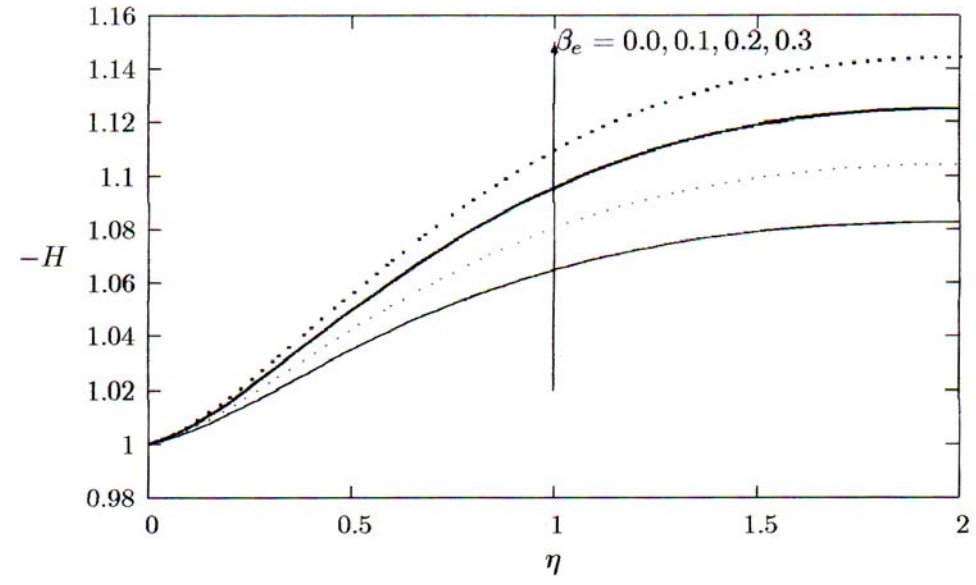

c

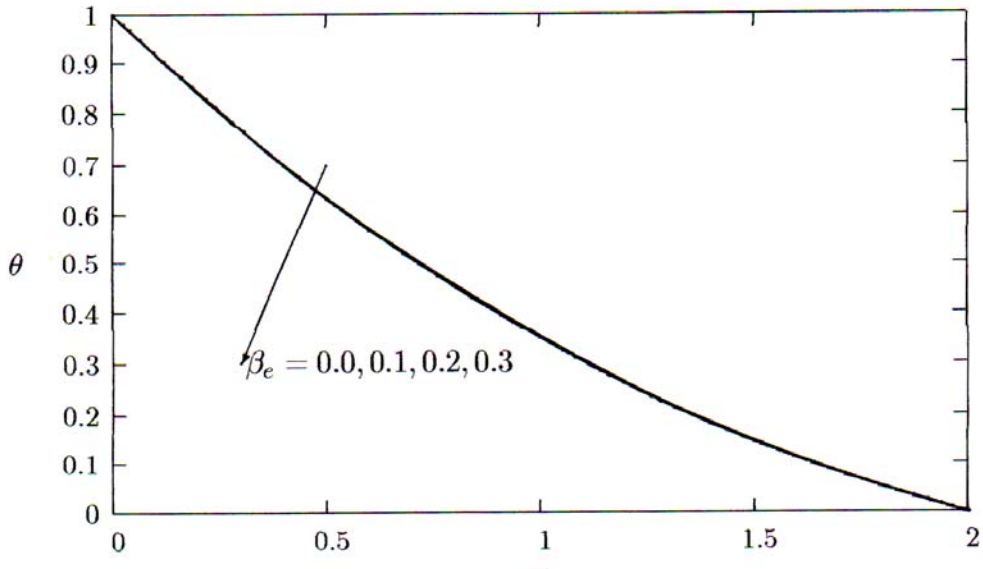

d

Fig. 5c,d – Effect of β_e on the axial velocity profiles (c) and on the temperature profiles (d), for: Ec = 0.2, Pr = 0.72, $\gamma = 0.1$, $M = 1$, $\beta_i = 0.1$, B = 0.1, and $W = -1$.

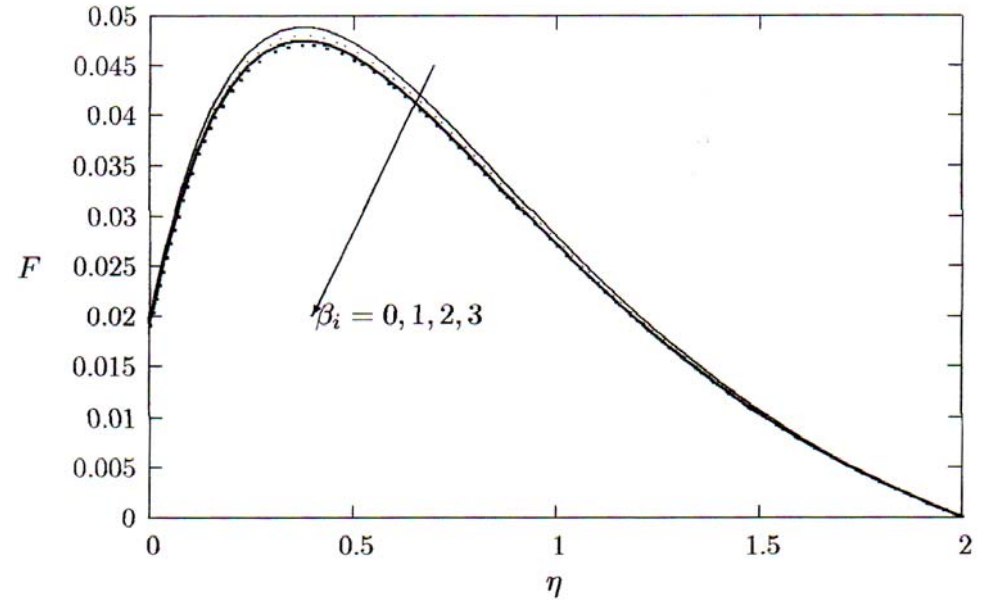

a

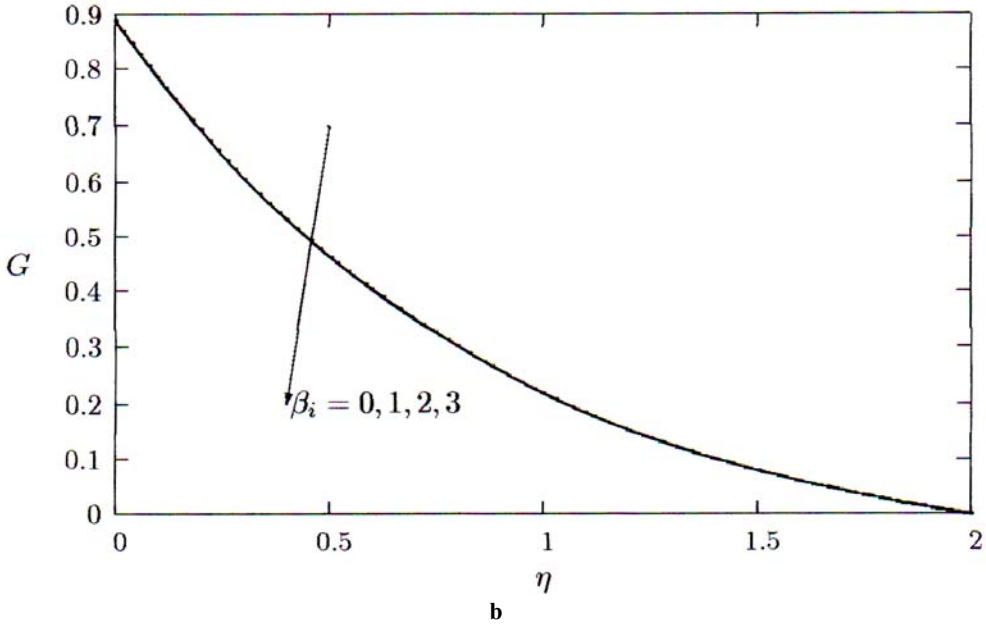

b

Fig. 6a,b – Effect of β_i on the radial velocity profiles (a) and on the tangential velocity profiles (b), for: Ec = 0.2, Pr = 0.72, $\gamma = 0.1$, $\beta_e = 0.1$, $M = 1$, B = 0.1, and $W = -1$.

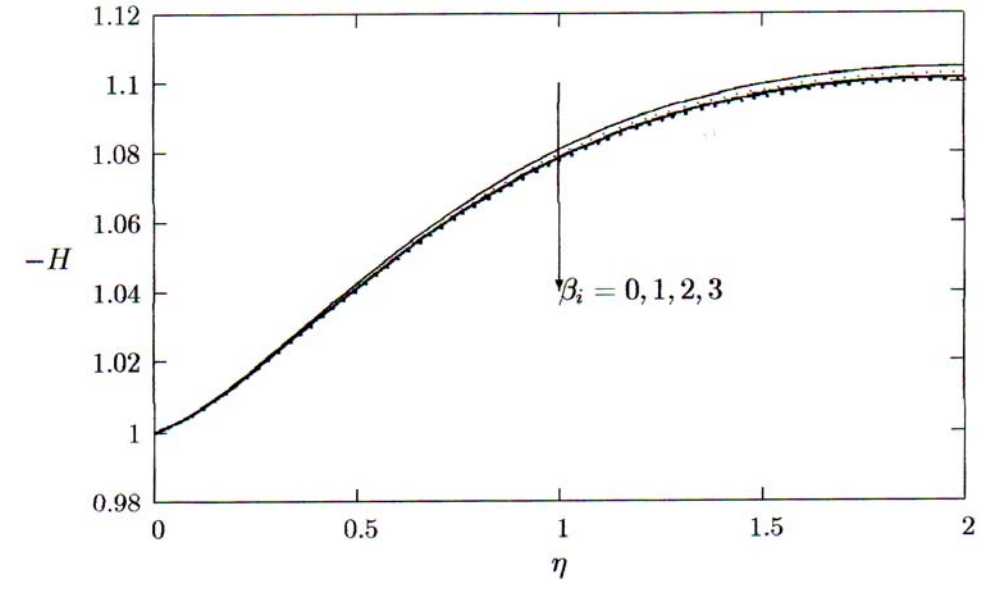

c

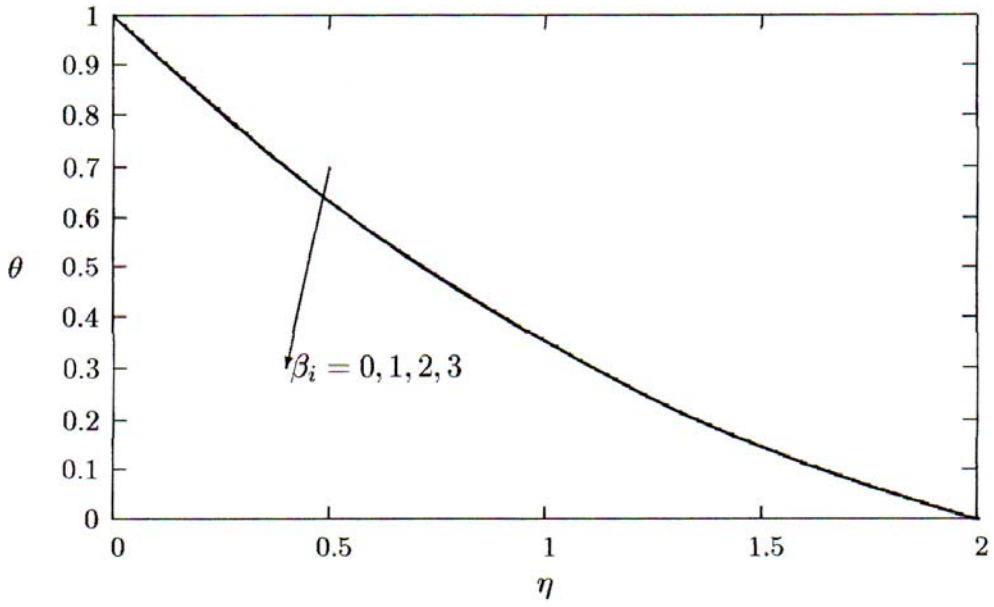

d

Fig. 6c,d – Effect of β_i on the axial velocity profiles (c) and on the temperature profiles (d), for: Ec = 0.2, Pr = 0.72, γ = 0.1, β_e = 0.1, M = 1, B = 0.1, and W = –1.

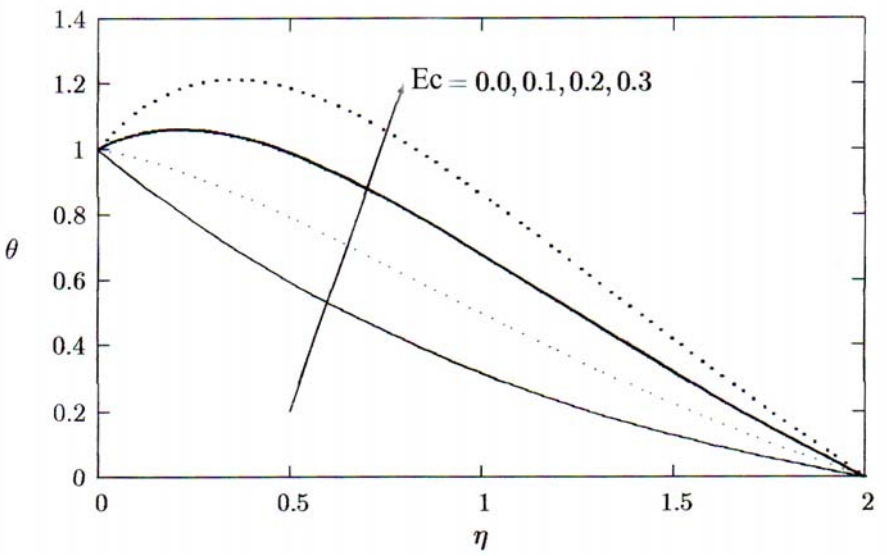

Fig. 7 – Effect of Ec on the on the temperature profiles for:
Ec = 0.2, Pr = 0.72, $\gamma = 0.1$, $\beta_e = 0.1$, $M = 1$, $\beta_i = 0.1$, B = 0.1, and $W = -1$.

6. CONCLUSIONS

In this study we have examined the effects of viscous dissipation and Joule heating on steady hydromagnetic and slip flow of a Bingham fluid over a porous rotating disk in the presence of Hall and ion-slip currents. Employing von Karman similarity transformation technique, the governing equations are transformed into ordinary differential equations and solve numerically by the shooting method. We present results to illustrate the flow characteristics for the velocity and temperature fields as well as the skin friction and rate of heat transfer, and show how the flow fields are influenced by the material parameters of the flow problem. We can conclude from our results that slip factor γ and Bingham number B has significant effects on the flow behaviour. We noticed that slip factor decreases radial, tangential and axial velocity components while it increases the temperature. Also, Bingham number decreases the magnitude of the radial and axial velocity components, skin frictions and rate of heat transfer, and increases the magnitude of the tangential velocity component and temperature. We also discovered that an increase in Hall parameter β_e, ion-slip parameter β_i decrease the temperature profiles while an increase in magnetic parameter and Eckert number decrease the rate of heat transfer coefficient.

Acknowledgement. This work is based upon work funded by TOTAL E&P (UK) for PhD studentship research in Marine Renewable Energy in the Institute of Petroleum Engineering, Heriot-Watt University, UK.

REFERENCES

1. T. von Karman, *Uber laminare und turbulente Reibung*, Z. Angew. Math. Mech., **1**, 233–255 (1921).
2. P.J. Zandbergen, D. Dijksra, *Von Karman swirling flows*, Ann. Rev. Fluid Mech., **19**, 465–491 (1987).
3. E. M. Sparrow, G. S. Beavers, L. Y. Hung, *Flow about a porous-surface rotating disk*, Int. J. Heat Mass Transfer, **14**, 993–996 (1971).
4. P. Mitschka, J. Ulbrecht, *Nicht-Newtonsche Flussigkeiten. IV. Stromung Nicht-Newtonsche Flussigkeiten Ostwarld-de Waelescher Typs in der Umebung Rotierender Drehkegel und Schieben*, Coll. Czech. Chem. Comm., **30**, 2511–2526 (1965).
5. G. C. Vradis, J. Dougher, S. Kumar, *Entrance pipe flow and heat transfer for a Bingham plastic*, Int. J. Heat Mass Transfer, **96**, 543–550 (1993).
6. E. C. Bingham, H. Green, *Plastic material and not viscous liquid; the measurement of its mobility and yield value*, Proc. Amer. Soc. Test Mater., **20**, *2*, 640–675 (1919).
7. Q. D. Nguyen, D. V. Boger, *Measuring the flow properties of yield stress fluids*, Annu. Rev. Fluid Mech., **24**, 47–88 (1992).
8. R. B. Bird, G. C. Dai, B. J. Yarusso, *The rheology and flow of viscoplastic materials*, Rev. Chem. Engng., **1**, 36–69 (1983).
9. I. C. Walton, S. H. Bittleston, *The axial flow of a Bingham plastic in a narrow eccentric annulus*, J. Fluid Mech., **222**, 39–60 (1991).
10. N Patel, D. B. Ingham, *Mixed convection flow of a Bingham plastic in an eccentric annulus*, Int. J. Heat Flow, **15**, *2*, 132–141 (1994).
11. T. Min, J. Y. Yoo, H. Choi, *Laminar convective heat transfer of a Bingham plastic in a circular pipe. II. Numerical approach-hydrodynamically developing flow and simultaneously developing flow*, Int. J. Heat Mass Transfer, **40**, *15*, 3689–3701 (1997).
12. A. G. Petrov, *The development of the flow of viscous and viscoplastic media between two parallel plates*, J. Appl. Math. Mech., **64**, *1*, 123–132 (2000).
13. S. Matsumoto, Y. Takashima, *Film thickness of a Bingham liquid on a rotating disk*, Ind. Eng. Chem. Fundam., **21**, 198–202 (1982).
14. A. A. Rashaida, *Flow of a non-Newtonian Bingham plastic fluid over a rotating disk*, PhD Thesis, University of Saskatchewan, 2005.
15. A.A. Rashaida, D. J. Bergstrom, R. J. Sumner, *Mass transfer from a rotating disk to a Bingham fluid*, ASME Applied Mechanics Division, **73**, 108–111 (2006).
16. G. W. Sutton, A. Sherman, *Engineering Magnetohydrodynamics*, McGraw-Hill, New York, 1965.
17. P. Mitschka, *Nicht-Newtonsche Flussigkeiten. II. Drehstomungen Ostwarld-deWaelescher Nicht-Newtonscher Flussigkeiten*. Coll. Czech., Chem. Comm., **29**, 2892–2905 (1964).
18. E. Osalusi, P. Sibanda, *On variable laminar convective flow properties due to a porous rotating disk in a magnetic field*, Romanian Journal of Physics, **51**, *9–10*, 933–944 (2006).
19. F. Frusteri, E. Osalusi, *On MHD and slip flow over a rotating porous disk with variable properties*, Accepted for publication in the Int. Comm. Heat and Mass Transfer, 2007.
20. M. Miklavcic, C. Y.Wang, *The flow due to a rough rotating disk*, Z. Angew. Math. Phys., **55**, 235–246 (2004).
21. M. Gad-el-Hak, *The fluid mechanics of microdevices-the Free Scholar Lecture*, J. Fluid Eng-T. Asme, **121**, 5–33 (1999).
22. A. Arikoglu, I. Ozkol, *On the MHD and slip flow over a rotating disk with heat transfer*, Int. J. of Numerical Methods for Heat and Fluid Flow, **28**, *2*, 172–184 (2006).